Received: 21 July 2023 | Revised: 7 December 2023 | Accepted: 6 January 2024

DOI: 10.1002/mop.34030

RESEARCH ARTICLE

WILEY

Miniaturized IPD bandpass filter design with high out-of-band rejection for 5G applications

Mingzhao Xu | **Yazi Cao** | **Yuhan Cao** | **Yanzhu Qi** | **Bo Yuan** | **Gaofeng Wang**

MOE Engineering Research Center of Smart Microsensors and Microsystems, School of Electronics and Information, Hangzhou Dianzi University, Hangzhou, China

Correspondence
Yazi Cao and Bo Yuan, MOE Engineering Research Center of Smart Microsensors and Microsystems, School of Electronics and Information, Hangzhou Dianzi University, Hangzhou, China.
Email: caoyazi@hdu.edu.cn and yuanbo@hdu.edu.cn

Funding information
Zhejiang Provincial Key Research & Development Project, Grant/Award Number: 2021C01041; National Key Research and Development Program of China, Grant/Award Number: 2019YFB2205003; National Natural Science Foundation of China, Grant/Award Numbers: 92373202, 62141409

Abstract

This letter proposes a miniaturized integrated passive device (IPD) bandpass filter (BPF) design with high out-of-band rejection for 5G applications. In this design, a novel topology based on the modified high-pass filter cascaded with the modified low-pass filter is introduced with two pairs of transmission zeros (TZs) at high and low frequencies. In addition, one grounded capacitor at the input is added to improve the suppression at high frequency end. The proposed BPF design is fabricated on silicon substrate. The measured insertion loss is around 3 dB and the return loss is <16 dB in the whole frequency range from 3.3 to 4.2 GHz for 5G applications. This proposed BPF achieves more than 20 dB sideband suppression at both stop bands from DC to 2.69 GHz and from 5.3 to 14 GHz. The fabricated device has a size of only $1 \times 0.7 \times 0.2$ mm.

KEYWORDS

bandpass filter (BPF), high out-of-band rejection, integrated passive device (IPD)

1 | INTRODUCTION

With rapid development of 5G wireless communication system, there is a strong demand for bandpass filter (BPF) with compact size, high out-of-band rejection, and low insertion loss to address spectrum congestion. However, achieving high performance in such a compact size is still a rather tough task. Integrated passive device (IPD) technology is a promising one to achieve high performance in a very compact circuit size.[1]

A novel method to design a BPF from an intertwined circular spiral inductor was proposed.[2] Moreover, a design methodology using π-type unit with inductive loading on integrated passive device has also been proposed.[3] In addition, a glass integrated passive device bandpass filter using synthesized stepped impedance resonators was presented.[4] However, all the proposed approaches cannot effectively control the out-of-band rejection and the steepness of the passband edges of the bandpass filters. To enhance the out-of-band rejection of the bandpass filters, there are some effective methods by adding transmission zeros (TZs).[1,5,6] In Reference,[5] stepped-impedance stubs embedded in coupled lines are used to introduce TZs on both sides of the filter passband and improve the selectivity. However, the device sizes were relatively large since the LTCC technology was used. In addition to adding TZs to the filter, increasing the filter order is also an effective way to improve the filter performance.[1,6] In Reference,[6] stepped-impedance multimode resonator is employed to achieve an ultra-wide upper stopband

attenuation. In Reference,[1] a hybrid resonant cavity technique, which produces six TZs in the stopband, was used to greatly improve the filter selectivity. Another way to improve out-of-band rejection is to add an additional filter circuit.[7–9] In references,[7,8] a TZ was introduced to improve out-of-band rejection by adding pi-type circuits to the output port of the filter. In reference,[9] TZs were introduced by using lumped-element bisected-pi sections at the filter input/output. In addition, adding cross coupling is also a general method to improve out-of-band rejection.[10]

In this letter, a design of miniaturized silicon-based IPD BPF with high out-of-band rejection is proposed. In this design, two pairs of TZs are introduced at high and low frequencies based on the cascade of the improved high-pass filter and low-pass filter. To improve the suppression of high frequencies, a ground capacitor is added at the input to improve the suppression at high frequency. In the following sections, band-pass filters using improved high-pass filters versus low-pass filters will be analyzed. The simulation results from the electromagnetic (EM) simulator UltraEM[11] as well as the measured results are included to illustrate and validate the proposed design.

2 | DESIGN AND ANALYSIS

A BPF can be constructed by a direct cascade of a low-pass filter (LPF) and a high-pass filter (HPF). Both upper and lower transition bands can be determined separately if the input and output impedances of the two filters are matched. To improve the performance of the upper and lower stopband, a novel topology based on the improved high-pass filter cascaded with the low-pass filter is herein introduced.

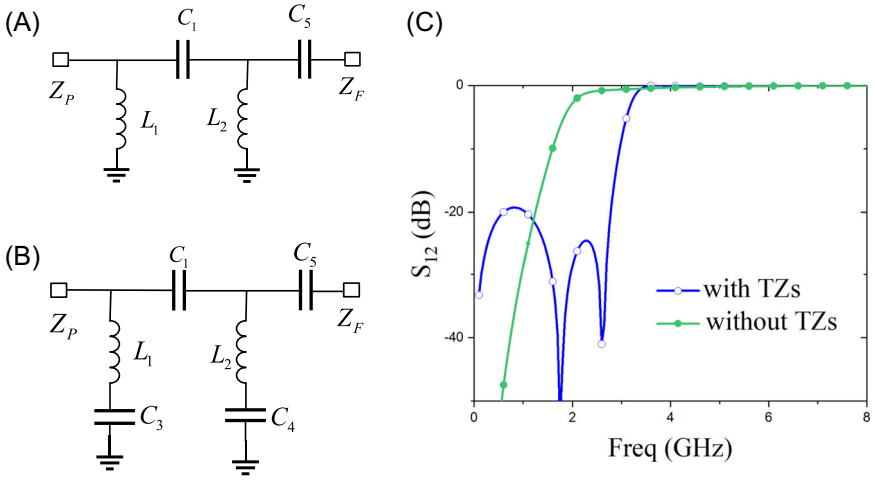

FIGURE 1 Simulated results of lumped high-pass filter circuit for the TZ. (A) Conventional lumped high-pass filter. (B) Proposed lumped high-pass filter. (C) Simulated frequency response curves of lumped high-pass filter. The values of the proposed lumped high-pass filter are listed as: $C_1 = 0.78$ pF, $C_3 = 3.13$ pF, $C_4 = 1.25$ pF, $C_5 = 1.65$ pF, $L_1 = 2.6$ nH, $L_2 = 2.94$ nH.

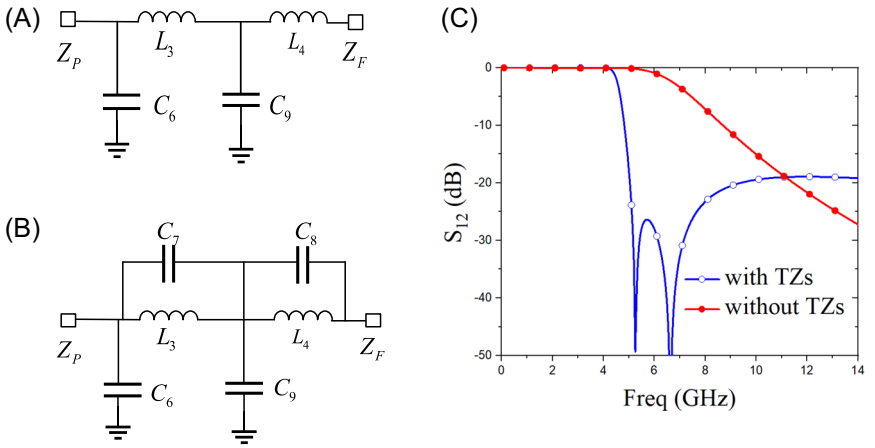

FIGURE 2 Simulated results of lumped low-pass filter circuit for the TZ. (A) Conventional lumped low-pass filter. (B) Proposed lumped low-pass filter. (C) Simulated frequency response curves of lumped low-pass filter. The values of the proposed lumped low-pass filter are listed as: $C_6 = 0.53$ pF, $C_7 = 0.3$ pF, $C_8 = 1.06$ pF, $C_9 = 0.94$ pF, $L_3 = 1.89$ nH, and $L_4 = 0.86$ nH.

2.1 | Modified high-pass filter topology

The traditional fourth order high pass filter is shown in Figure 1A, to achieve high out-band suppression at the low frequency range, one modified topology is introduced as shown in Figure 1B. Compared with traditional high pass filter, L_1 and L_2 are connected in series with C_3 and C_4 respectively. It can generate two TZs at low frequencies to improve out of band suppression at 1.7 and 2.69 GHz. To verify the proposed topology, the simulation with C_3 and C_4 is compared with that without C_3 and C_4.

To analyze the proposed filter topology, the ABCD matrix of its two ports network can be written as

$$\begin{pmatrix} A & B \\ C & D \end{pmatrix} = \begin{pmatrix} 1 & 0 \\ jB_1 & 1 \end{pmatrix}\begin{pmatrix} 1 & -jX_1 \\ 0 & 1 \end{pmatrix}\begin{pmatrix} 1 & 0 \\ jB_2 & 1 \end{pmatrix}\begin{pmatrix} 1 & -jX_2 \\ 0 & 1 \end{pmatrix} = \begin{pmatrix} 1 + X_1B_2 & -jX_2 - jX_1X_2B_2 - jX_1 \\ jB_1 + jX_1B_1B_2 + jB_2 & X_2B_1 + X_1X_2B_1B_2 + B_2X_2 + X_1B_1 + 1 \end{pmatrix}, \tag{1}$$

where $B_1 = \frac{\omega C_3}{1-\omega^2 L_1 C_3}$, $B_2 = \frac{\omega C_4}{1-\omega^2 L_2 C_4}$, $X_1 = \frac{1}{\omega C_1}$, $X_2 = \frac{1}{\omega C_5}$, ω is the TZ frequency of the filter. Two port network equivalent circuit, parameter conversion of S parameter to ABCD matrix:

$$S_{12} = \frac{2(\mathrm{AD} - \mathrm{BC})}{A + B/Z_0 + \mathrm{CZ}_0 + D}, \tag{2}$$

$$S_{21} = \frac{2}{A + B/Z_0 + \mathrm{CZ}_0 + D}. \tag{3}$$

Once the frequency of $S_{12} = 0$ is determined, the values of ω_1 and ω_2 can be calculated as

$$\begin{cases} \omega_1 = 1/\sqrt{L_1C_3} \\ \omega_2 = 1/\sqrt{L_2C_4} \end{cases}, \tag{4}$$

where $C_3 = 3.13$ pF, $C_4 = 1.25$ pF, $L_1 = 2.6$ nH, $L_2 = 2.95$ nH in our proposed design. The position of two TZs can be calculated, $f_1 = 1.76$ GHz, $f_2 = 2.62$ GHz.

2.2 | Modified low-pass filter topology

The traditional fourth order high pass filter is shown in Figure 2A, to achieve high out band suppression at the high frequency range, one modified topology is introduced as shown in Figure 2B. Compared with the traditional high pass filter, C_7 and C_8 are connected in parallel through L_3 and L_4 respectively, and two TZs are introduced to improve the out of band suppression of low frequency 5.15 and 7 GHz. To verify the proposed topology, the simulation with C_7 and C_8 is compared with that without C_7 and C_8.

To analyze the proposed low-pass filter, the ABCD matrix of its two-port network can be written as

$$\begin{pmatrix} A & B \\ C & D \end{pmatrix} = \begin{pmatrix} 1 & 0 \\ jB_3 & 1 \end{pmatrix}\begin{pmatrix} 1 & jX_3 \\ 0 & 1 \end{pmatrix}\begin{pmatrix} 1 & 0 \\ jB_4 & 1 \end{pmatrix}\begin{pmatrix} 1 & jX_4 \\ 0 & 1 \end{pmatrix} = \begin{pmatrix} 1 - X_3B_4 & jX_4 - jX_3X_4B_4 + jX_3 \\ jB_3 - jX_3B_3B_4 + jB_4 & -X_4B_3 + X_3X_4B_3B_4 - B_4X_4 - X_3B_3 + 1 \end{pmatrix}, \tag{5}$$

where $X_3 = \frac{\omega L_3}{1-\omega^2 L_3 C_7}$, $X_4 = \frac{\omega L_4}{1-\omega^2 L_4 C_8}$, $B_3 = \omega C_6$, $B_4 = \omega C_9$, ω is the TZ frequency of the filter. According to Equations (2) and (5), two TZs are solved, the values of ω_3 and ω_4 can be calculated as

$$\begin{cases} \omega_3 = 1/\sqrt{L_3C_7} \\ \omega_4 = 1/\sqrt{L_4C_8} \end{cases}, \tag{6}$$

where $C_7 = 0.3$ pF, $C_8 = 1.06$ pF, $L_3 = 1.89$ nH, $L_4 = 0.86$ nH in our proposed design. The position of two TZs can be calculated, $f_3 = 6.68$ GHz, $f_4 = 5.27$ GHz.

2.3 | Proposed BPF topology

In this paper, a novel topology based on the modified high-pass filter cascaded with the modified low-pass filter is introduced here. In additional, to further improve the stopband rejection and selectivity affected by the parasitic parameters, a grounded capacitor is introduced at the input, as shown in Figure 3A. This new added grounded capacitor can greatly enhance the out of band

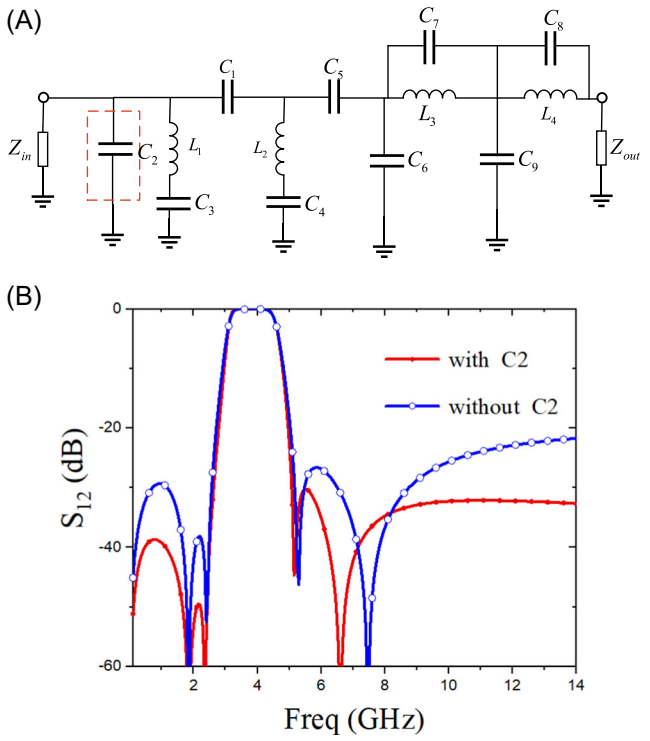

FIGURE 3 (A) The schematic of proposed BPF. (B) Simulated results of lumped bandpass filter with or without C_2. The values of the proposed lumped bandpass filter are listed as: $C_1 = 0.48$ pF, $C_2 = 0.96$ pF, $C_3 = 4.06$ pF, $C_4 = 0.74$ pF, $C_5 = 0.13$ pF, $C_6 = 0.03$ pF, $C_7 = 0.07$ pF, $C_8 = 0.82$ pF, $C_9 = 0.49$ pF, $L_1 = 1.82$ nH, $L_2 = 6.12$ nH, $L_3 = 7.73$ nH, and $L_4 = 1.15$ nH.

suppression of 10 GHz. To verify the proposed topology, the results with and without this added grounded capacitor is also compared and analyzed. Through the circuit optimization, the theoretical values of BPF circuit without C_2($C_1 = 0.6$ pF, $C_3 = 2.29$ pF, $C_4 = 1.03$ pF, $C_5 = 0.28$ pF, $C_6 = 0.11$ pF, $C_7 = 0.1$ pF, $C_8 = 1.13$ pF, $C_9 = 0.81$ pF, $L_1 = 3.25$ nH, $L_2 = 4.19$ nH, $L_3 = 4.42$ nH, and $L_4 = 0.8$ nH) can be calculated as initial values for operation band. Here the grounded capacitor C_2 is added to increase the suppression at stopband. The values of the BPF circuit are further optimized, as shown in Figure 3B. The structure with parallel capacitor is provided, and the suppression level increases sharply by at least 10 dB above 10 GHz.

3 | PROTOTYPE AND EXPERIMENTAL RESULTS

The proposed IPD BPF design is implemented using the thin-film process technology on High Resistivity Silicon (HRS) substrate. The cross section is illustrated in Figure 4A. The HRS substrate has thickness of 200 μm. It provides two metal layers (Cu) and dielectric layers consisting of oxides and SiN. The relative permittivity values for HRS, SiN, and oxides are 11.9, 7, and 4, respectively. Through this thin-film technology, it is possible to fabricate inductors and capacitors.

In Figure 4C depicts the results of a group of EM simulations. Compared with the BPF without TZs, the BPF shows better selectivity. However, due to the influence of parasitic parameters of lumped elements, the out of band suppression at frequencies above 10 GHz becomes worse. By introducing a grounding capacitor, it is confirmed that the out of band suppression at high frequencies can be enhanced. The detailed dimensions of octagonal inductors and metal-insulator-metal (MIM) capacitors in Figure 3A are listed in Table 1.

Based on the above analysis, the proposed BPF is simulated and its GDS layout is generated by EM simulator UltraEM from Faraday Dynamics, Inc11. The IPD layout and the micrograph of the proposed silicon-based BPF design is shown in Figure 4B,D, respectively.

The fabricated BPF is measured on-chip using the Keysight N5244A PNA-X vector network analyzer and Cascade summit-11000 probe station. The simulated and measurement results of the proposed BPF are compared in Figure 4E. The simulation results are in good agreement with the measured ones. In the operating band (i.e., 3.3~4.2 GHz), it achieves insertion loss around 2.7 dB and return loss below 16 dB. In addition, it has ultrahigh out-of-band rejection and ultra-wide upper resistance band. Specifically, its out-of-band rejection is better than 25 dB (even better than 40 dB in a partial range) at the low frequency band from DC to 2.69 GHz and better than 19 dB at the high frequency band from 5.3 to 14 GHz. In Figure 4F depicts the results of a group of simulated and measured group delay. The group delay of the filter is within 1 ns in the passband. From the results, the group delay of the filter based on the IPD process has a relatively small impact on the system. There are some minor frequency shifts between the simulated and measured results due to the manufacturing tolerances. Compared to the previous design shown in Table 2, the proposed filter offers an exceptionally ultra-wide out-of-band rejection, surpassing references.[4,5,12] Moreover, this proposed filter exhibits more TZs compared to references,[3,4,7,12] thereby significantly enhancing its selectivity and passband edge steepness. In addition, the proposed BPF exhibits smaller electrical size than previous designs, which makes it suitable for integrating with 5G radio frequency (RF) front-end systems.

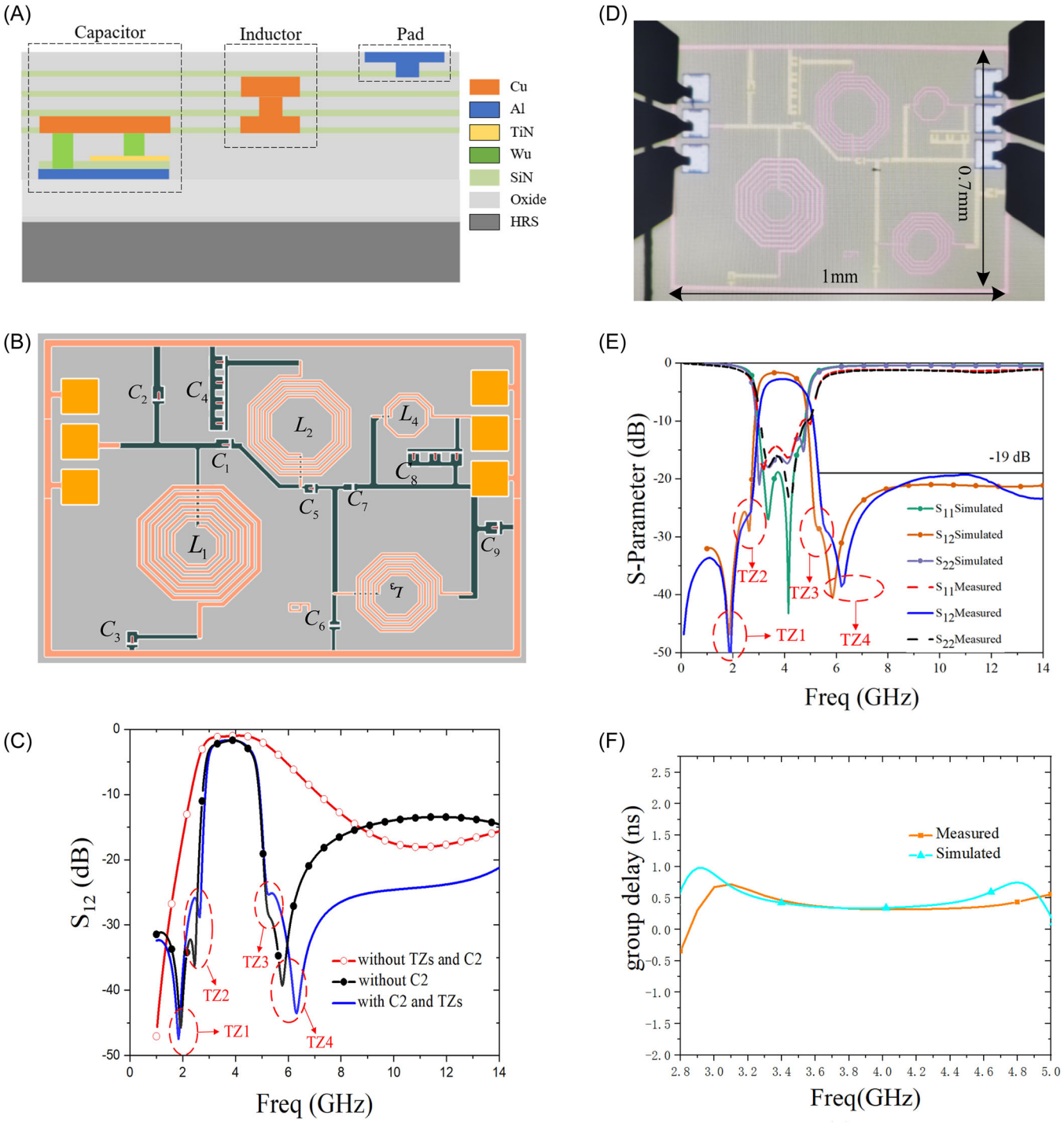

FIGURE 4 (A) Cross-sectional view of the HRS-based IPD. (B) Chip layout view. (C) Simulated results of the BPFs. (D) Micrograph of the proposed BPF. (E) Simulated and measured results of the proposed BPF. (F) Simulated and measured group delay results of the BPFs.

Inductor	Inner diameter (μm)	Width (μm)	Space (μm)	Number of turns
L_1	80	6.5	5	6.5
L_2	128	6	5	4.5
L_3	86	6	5	4.5
L_4	75	6	5	1.5
Capacitor	**Length (μm)**			**Width (μm)**
C_1	30			21
C_2	30			24.4
C_3	30			85.32
C_4	30			29.1
C_5	20			19.85
C_6	10			22.1
C_7	20			15
C_8	30			72.23
C_9	27			28.73

TABLE 1 Fabricated dimensions of elements in the proposed BPF.

TABLE 2 Comparison of the proposed BPF with several reported BPF.

References	f_0 (GHz)	Insertion loss (dB)	Size (λ_0^2) × 10^{-4}	Return loss (dB)	TZs	19-dB rejection	Process
[3]	4	2.12	3.2 × 0.8	14.8	2	11.25 f_0	GaAs
[4]	3	3.1	1.55 × 0.92	18	2	-	GaAs
[5]	3.5	2.3	7 × 8	12.8	4	2.2 f_0	LTCC
[7]	3.35	2.05	1.675 × 0.67	19	3	12 f_0	GaAs
[12]	8	2.92	6.1 × 5.4	16.1	0	2.5 f_0	Si
This work	3.75	2.7	1.25 × 0.875	16	4	3.8 f_0	HRS

Abbreviations: TZs, transmission zeros near the passband, λ_0, the wavelength in air at f_0.

4 | CONCLUSION

In this letter, a miniaturized BPF design with high out-of-band rejection and low insertion loss has been presented. The improved high-pass filter cascaded with the low-pass filter was introduced in the proposed BPF design. The proposed BPF design was fabricated on silicon substrate. The measured results are in good agreement with the simulated results. The BPF has a bandwidth coverage from 3.3 to 4.2 GHz, with insertion loss of around 3.0 dB and return loss of less than 16 dB. In addition, the filter achieves very steep low-band edges and impressive out-of-band rejection. It has ultrahigh out-of-band rejection and ultra-wide upper resistance band. Specifically, its out-of-band rejection is better than 25 dB (even better than 40 dB in a partial range) at the low frequency band from DC to 2.69 GHz and better than 19 dB at the high frequency band from 5.3 to 14 GHz. The fabricated BPF device has a miniaturized size of 1 × 0.7 mm, which can be used in 5G applications.

ACKNOWLEDGMENTS

This work was supported by National Natural Science Foundation of China under Grant 62141409, National Key Research and Development Program of China under Grant 2019YFB2205003, and Zhejiang Provincial Key Research & Development Project under Grant 2021C01041.

DATA AVAILABILITY STATEMENT

Data sharing not applicable to this article as no data sets were generated or analyzed during the current study.

ORCID

Bo Yuan http://orcid.org/0000-0001-5045-7584
Gaofeng Wang http://orcid.org/0000-0001-8599-7249

REFERENCES

1. Hu X-J, Yang T. A compact 5G band N77 bandpass filter with multiple zeros based on GaAs integrated passive device process. *Microw Opt Technol Lett*. 2023;65(6):1589-1594.
2. Wang Z-J, Kim E-S, Liang J-G, Kim N-Y. QFN-packaged bandpass filter with intertwined circular spiral inductor and integrated center-located capacitors using integrated passive device technology. *IEEE Access*. 2019;7(6):13597-13607.
3. Liu B-G, Zhou Y-J, Cheng C-H. Miniaturized ultra-wideband bandpass filter with ultra-wide stopband using π-type unit with inductive loading on integrated passive device. *IEEE Trans Circuits Syst II Express Briefs*. 2021;68(11):3406-3410.
4. Chen F-J, Cheng X, Zhang L, Tian Y-L, Tang Y, Deng X-J. Synthesis and design of lumped-element filters in GaAs technology based on frequency- dependent coupling matrices. *IEEE Trans Microwave Theory Tech*. 2019;67(4):1483-1495.
5. Zhao W, Wu Y, Yang Y, Wang W. LTCC bandpass filter chips with controllable transmission zeros and bandwidths using stepped-impedance stubs. *IEEE Trans Circuits Syst II Express Briefs*. 2022;69(4):2071-2075.
6. Lyu Y-P, Zhou Y-J, Zhu L, Cheng C-H. Compact and high-order on-chip wideband bandpass filters on multimode resonator in integrated passive device technology. *IEEE Electron Device Lett*. 2022;43(2):196-199.
7. Luo X-H, Cheng X, Zhang L, et al. A miniaturized on-chip BPF with ultrawide stopband based on lumped Pi-section and source-load coupling. *IEEE Microw Wirel Compon Lett*. 2019;29(29):516-519.
8. Jiang Y, Feng L-P, Zhu H-S, et al. Bandpass filter with ultra-wide upper stopband on GaAs IPD technology. *IEEE Trans Circuits Syst II Express Briefs*. 2022;69(2):389-393.
9. Marin S, Martinez JD, Valero CI, Boria VE. Microstrip filters with enhanced stopband based on lumped bisected Pi-sections with parasitics. *IEEE Microw Wirel Compon Lett*. 2017;27(1):19-21.
10. Wu WJ, Yuan B, Zhao W-S, Wang G. On-chip miniaturized bandpass filter using gallium arsenide-based integrated passive device technology. *Microw Opt Technol Lett*. 2022;64(4):688-693.
11. UltraEM V202109. Faraday Dynamics, Inc.; 2022.
12. Huang C-C, Fang W-T, Lin Y-S. Miniaturization of broadband stub bandpass filters using bridged-T coils. *IEEE Access*. 2018;6(9):20164-20173.

How to cite this article: Xu M, Cao Y, Cao Y, Qi Y, Yuan B, Wang G. Miniaturized IPD bandpass filter design with high out-of-band rejection for 5G applications. *Microw Opt Technol Lett*. 2024;66:e34030. doi:10.1002/mop.34030